Journal of Materials Chemistry B

PAPER

View Article Online
View Journal | View Issue

Cite this: J. Mater. Chem. B, 2014, 2, 2240

Folic acid-conjugated glucose and dextran coated iron oxide nanoparticles as MRI contrast agents for diagnosis and treatment response of rheumatoid arthritis

Fengying Dai,[a] Meihong Du,[b] Yingguo Liu,[a] Guiying Liu,*[c] Qingjun Liu*[b] and Xin Zhang*[a]

Received 6th December 2013
Accepted 24th January 2014

DOI: 10.1039/c3tb21732a

www.rsc.org/MaterialsB

Coating superparamagnetic iron oxide (SPIO) with dextran increases the stability of the magnetic nanoparticles during blood circulation, yet this is accompanied by an increase in the particle size and the vascular permeability efficiency of the SPIO nanoparticles into the joints decreases. In our study, the thickness of the dextran coated onto SPIO (dex-SPIO) was optimized without affecting the magnetic quality of iron oxide by adding a suitable amount of glucose into the crystal growth process. To further improve the signal enhancement effect of this glucose and dextran coated SPIO (glu-dex-SPIO) for the detection of the inflammatory site of arthritis, folic acid (FA) was conjugated to glu-dex-SPIO. This FA glu-dex-SPIO was used as a negative contrast agent for MRI to visualize the antigen induce arthritis (AIA) model in rats using a 7 T MR scans. MR imaging revealed more significant differences between the synovium and surrounding tissues with FA glu-dex SPIO than when using the non-targeting glu-dex-SPIO over a long period of time (24 h) after intravenous injection. Moreover, the therapeutic efficacy of the cyclooxygenase 2 (COX-2) inhibitor treatment of the inflamed joints also could be confirmed by using FA glu-dex SPIO enhanced MRI, indicating that this type of nanoparticles could also have potential as a contrast agent for measuring the treatment response of rheumatoid arthritis.

1 Introduction

Rheumatoid arthritis (RA) is a systemic inflammatory autoimmune disease characterized by chronic inflammation and subsequent joint destruction. Until recently, there had been little hope for patients with rheumatoid arthritis. The current methods for RA treatment have been restricted to inflammation control and the prevention of joint destruction, rather than a complete disease cure. Therefore, finding a proper recognition and therapy monitor for RA is crucial.[1–3] Traditionally, a major tool for diagnosing or monitoring the progression of joint destruction caused by RA has been radiography. A limitation lies in the fact that only the late signs of this progressive disease can be visualized by these radiography techniques, by then irreversible bone damage can not be avoided in a high proportion of patients.[4] Owing to its high spatial resolution and soft-tissue contrast, magnetic resonance (MR) imaging is considered to be the imaging modality of choice for soft tissue detail of joints rather than simple radiographs for the detection of rheumatoid arthritis.[5–7] Gadolinium or gadopentetate dimeglumine (Gd-DTPA) agents have frequently been preferred in MR diagnostic practice. Yet these gadolinium-containing T_1 contrast agents also have some disadvantages, such as raising toxicity and a short retention time in the vascular system. These limitations of gadolinium contrast agents have prompted the development of new contrast agents based on superparamagnetic iron oxide particles.[8]

Previous studies have shown that the biodistribution and vascular penetration of iron oxide nanoparticles depends on the size and thickness of the coating of the iron oxide contrast agent.[9] Ultrasmall superparamagnetic nanoparticles with a hydrodynamic diameter below 9 nm typically exhibit higher blood vessels penetration efficiency than larger nanoparticles.[10,11] Polymeric materials (*e.g.*, dextran) have been widely adopted to impart blood circulation stability upon iron oxide contrast agents in magnetic resonance imaging (MRI) of the liver.[12–14] Nevertheless, the addition of a dextran coating is always accompanied by an increase in the particle size and, thereby, inefficiency during the MRI of RA.[15,16] A proper design of a dextran coated iron oxide contrast agent for RA must take

[a]National Key Laboratory of Biochemical Engineering, Institute of Process Engineering, Chinese Academy of Sciences, Beijing 100190, P.R. China. E-mail: xzhang@home.ipe.ac.cn; Fax: +86 010 82544853; Tel: +86 010 82544853

[b]Beijing Center for Physical and Chemical Analysis, Beijing 100871, P.R. China. E-mail: Liuqj@bjast.ac.cn; Tel: +86 010 88417669

[c]Department of Pediatrics, Capital Medical University Affiliated Beijing Anzhen Hospital, Beijing 100029, P.R. China. E-mail: liugvying@126.com; Tel: +86 010 84005105

into consideration both the super small iron oxide core and the thin shell of the nanoparticles. Nevertheless, these two aspects are contradictory in a traditional co-precipitation method, as excess amount of dextran could be added to reduce the over growth of the iron oxide crystals, but this would necessarily increase the thickness of the outer layers to a certain extent.[17,18]

In order to improve the synthesis of dextran coated iron oxide nanoparticles with a view toward optimizing the thickness of the dextran coating and the magnetic response properties of the iron oxide cores, a simple one-step method that provides aqueous dispersions of glucose and dextran stabilized super paramagnetic iron oxide (SPIO) has been reported in the present work. Iron salts are precipitated in the presence of glucose (during the growth stage), which stabilizes the particles and provides significantly smaller nanoparticles compared to pure dextran coated SPIO nanoparticles. An adequate balance between the hydrodynamic diameter and super paramagnetic properties of the iron oxide colloid crystals can be achieved by regulating the glucose content during the iron oxide crystal growth stage. In order to further improve the signal enhancement effect of these glucose and dextran coated SPIO (glu-dex SPIO) nanoparticles for the detection of the inflammatory sites of arthritis, folic acid was conjugated to glu-dex SPIO for its specific binding to the recruited and activated macrophages of synovium in RA based on their overexpression of folic acid receptors.[19,20]

2 Materials and methods

2.1 Materials

Ferrous sulfate heptahydrate, ferric chloride hexahydrate, ammonium hydroxide and folic acid were purchased from Sigma-Aldrich. Dextran ($M_w = 7000$ Dalton) was purchased from Pharmacia, USA. 1-Ethyl-3-(3-dimethylaminopropyl)carbodiimide hydrochloride (EDC) and 4-dimethylaminopyridine (DMAP) were purchased from Alfa Aesar. Tumor necrosis factor-α (TNF-α) and interferon (γIFN) were purchased from Pepro Tech Company. Freund's complete adjuvant was obtained from the Sigma Chemical regent company. RAW264.7 cell, a mouse monocyte macrophage cell line, was purchased from Shanghai Fuxiang Technology Company Limited. All reagents were purchased from common commercial sources and used without further purification.

2.2 Synthesis procedure for the glu-dex SPIO magnetic nanoparticles

Aqueous dispersions of the glu-dex SPIO magnetic nanoparticles were prepared using a co-precipitation method. Ammonium hydroxide (35 mL) was added to a mixture of Fe(II) chloride and Fe(III) (molar ratio [Fe(II)]/[Fe(III)] = 0.5) containing ferrous sulfate heptahydrate (300 mg) and dextran (500 mg) in an aqueous solution. Crystal growth of the magnetite nanoparticles was allowed to continue for 30 min after the addition of a glucose solution with a final concentration of either 2 mg mL^{-1}, 5 mg mL^{-1} or 10 mg mL^{-1}. The reactor was degassed with nitrogen at 80 °C throughout the experiments. Four types of magnetic nanoparticles; dex-SPIO, glu-dex SPIO, glu-dex SPIO1 and glu-dex SPIO2 were synthesised using glucose concentration of 0 mg mL^{-1}, 2 mg mL^{-1}, 5 mg mL^{-1} and 10 mg mL^{-1}, respectively. These nanoparticles were isolated from solution by applying an external magnetic field, after the addition of a small quantity of ethanol into the solution. The magnetic particles were separated and washed three times and then dispersed in saline to form a magnetofluids for MR imaging.

2.3. Preparation of FA glu-dex SPIO

Folic acid (175 mg), DMSO (10 mL), EDC (8 mg) and DMAP (10 mg) were added into a bottle in sequential order and the mixture was shaken at 25 °C for 30 min. A glu-dex SPIO aqueous solution was then added into the reactor with continuous shaking at 25 °C for 24 h. The FA glu-dex SPIO was washed and isolated by magnetic separation. Afterwards, the cleaning process was repeat three times in order to remove any free folic acid.

2.4 Characterization of the SPIO

The crystal structures of the SPIO nanoparticles were studied using X-ray powder diffraction (XRD) with a Bruker D8 ADVANCE diffractometer. The average size of the crystals (D; nm) was estimated using Scherrer's formula. The particle core size and morphology were studied using TEM (JEM-2100 electron microscope) operating at an acceleration voltage of 200 kV. The hydrodynamic size and size distribution of SPIO were assessed using a dynamic light scattering (DLS) instrument (Malvern Zetasizer Nano ZS). The thermal stability and content of the coating materials of the SPIO nanoparticles were checked using thermogravimetric analysis (Mettler-Toledo, TGA/DSC1) with a heating rate of 10 °C min^{-1} in a N_2 flow. The magnetization curves of the magnetic particles were measured using a vibrating sample magnetometer (BHV-50HTI). The transverse relaxation properties of SPIO were measured with a Magnetic Resonance Analyzer (Bruker, minispec mq60). The X-ray photoelectron spectroscopy (XPS) of the SPIO nanoparticles was studied with a Thermo ESCALAB 250xi instrument.

2.5. Macrophagocyte cellular uptake experiments

RAW264.7 cells were seeded into a 24-well plate at a density of 5×10^5 cells per well in 500 μL of growth medium and incubated for 12 h. A TNF-α/γIFN solution was then applied to each well at a final concentration of γIFN (100 U mL^{-1}) and TNF-α (400 U mL^{-1}). The medium was removed after 24 h and replaced with a mixture of 500 μL growth medium and 10 μL SPIO (10 mg mL^{-1}). The plate was further incubated for 6 h, then all of the medium was discarded carefully and cells were washed three times with 500 μL of PBS. The cells were fixed with glutaraldehyde and then Prussian blue staining for the iron content assessment.

2.6. Induction of AIA

The AIA model was performed using methods previously reported in the literature.[21] Briefly, male Lewis rats (weighing 200 g) were injected subcutaneously in the paw with 0.1 mL of Freund's complete adjuvant. The joint swelling was quantified

by measuring perpendicularly with calipers. The skin thickness was measured and the results indicated antigen-induced arthritis.

2.7. *In vivo* MR imaging

The SPIO solutions were injected intravenously through the tail vein at a dose of 5 mg/200 g animal body weight. The AIA animal MR images were obtained with a 7 T MRI imager (Bruker Biospec 7 T) at 24 h post injection of SPIO. All of the animals were anaesthetized before imaging. For the MR imaging of the rats, T_2-weighted fast-spin-echo sequences were performed. The intragastric administration rats were fed with the same dose of COX every other day for 10 days. The control rats were treated with the same amount of saline. The rats were killed after the MR imaging with the ankle joints of the AIA rats collected for routine Hematoxylin–Eosin (H–E) and Prussian blue staining. All animal experiments were performed in compliance with the institutional ethics committee regulations and guidelines on animal welfare.

3. Result and discussion

3.1 Optimization of the magnetic properties of glucose and dextran coated SPIO

The typical method for the synthesis of dextran coated iron oxide nanoparticles is the co-precipitation of iron salts in the presence of an excess of dextran. An adequate balance between iron oxide core size and exterior hydrophilic layer thickness of dextran can not be achieved with a single adjustment of the amount of dextran. To optimize the synthesis of these SPIO particles with a view toward optimization of the thickness of the dextran coating and the magnetic response properties of the iron oxide core, glucose was introduced to increase the stability of the particles and this provides significantly smaller nanoparticles compared with pure dextran coated SPIO nanoparticles (Fig. 1A).

The hysteresis loops of the dex-SPIO and glu-dex SPIO nanoparticles were investigated in order to optimise the magnetic properties of the glucose and dextran coated SPIO. Fig. 1B shows the typical magnetization curves and hysteresis loops for the SPIO nanoparticles. Typical characteristic curves for dextran SPIO (dex-SPIO) and glucose and dextran coated SPIO (glu-dex SPIO) at a glucose concentration of 2 mg mL^{-1} were observed showing an almost immeasurable coercivity and remanence at room temperature, indicating the superparamagnetic nature of dex-SPIO and glu-dex SPIO. These superparamagnetic characteristics signified that these particles possessed single domains and all of the magnetic moments were aligned in one direction. Dex-SPIO and glu-dex SPIO exhibited M_s values of 45 and 42 electromagnetic units per gram (emu per g), respectively (Fig. 1B). Glucose, as a small polyhydroxy molecule, served as a chelating agent that controlled the iron oxide core size and could reduce the dextran exterior of SPIO in our study. However, the glucose method has to be carefully monitored in order to obtain a balance between the proper size and magnetic response performance of SPIO. As observed in Fig. 1B, when the glucose concentration increases to 5 mg mL^{-1} and 10 mg mL^{-1} during the iron oxide synthesis stage it can cause a loss in the saturation magnetization property and the reason for this could be the involvement of the glucose and iron atoms in a spin–lattice relaxation process. This effect is consistent with previous reports, which showed that reducing the particles to a limited size can lower their magnetic moment and, therefore, their outer-sphere relaxivity (r_2) due to a noncollinear spin arrangement near the surface.[15] Therefore, a suitable level of glucose capping of the glu-dex SPIO nanoparticles was intentionally selected in order to ensure an adequate balance between the hydrodynamic diameter and superparamagnetic properties of the iron oxide colloid crystals.

3.2 Size and morphology examination of the SPIO nanoparticles

TEM images show the morphology and mean diameter of the as synthesized iron oxide nanoparticles. They indicate that both the dex-SPIO and glu-dex SPIO nanoparticles are spherical with homogeneous size distributions (Fig. 2A and B). For dex-SPIO, the particles tend to be slightly larger and the mean core size is about 8.5 nm. As for dex-glu SPIO, it possesses an average core size of 4.6 nm. In agreement with the TEM results, the hydrodynamic diameter obtained using DLS also shows similar values where the mean hydrodynamic size of glu-dex SPIO was 9.1 ± 0.57 nm, while dex-SPIO had a significantly larger size of

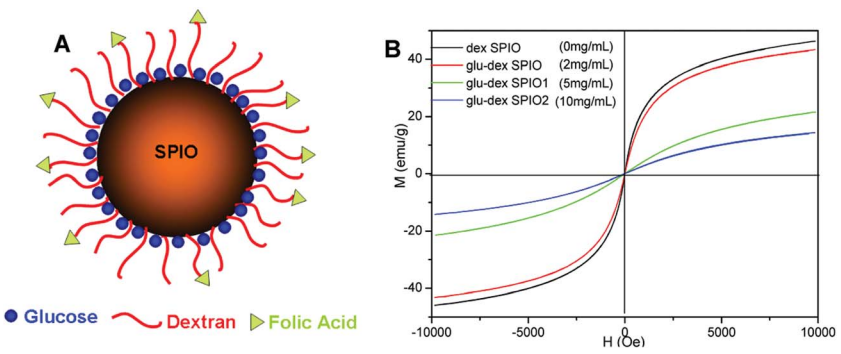

Fig. 1 A sketch of a glucose and dextran coated SPIO nanoparticle (A) and the magnetic hysteresis loops of dex-SPIO and glu-dex SPIO nanoparticles obtained using a series of glucose concentrations (B).

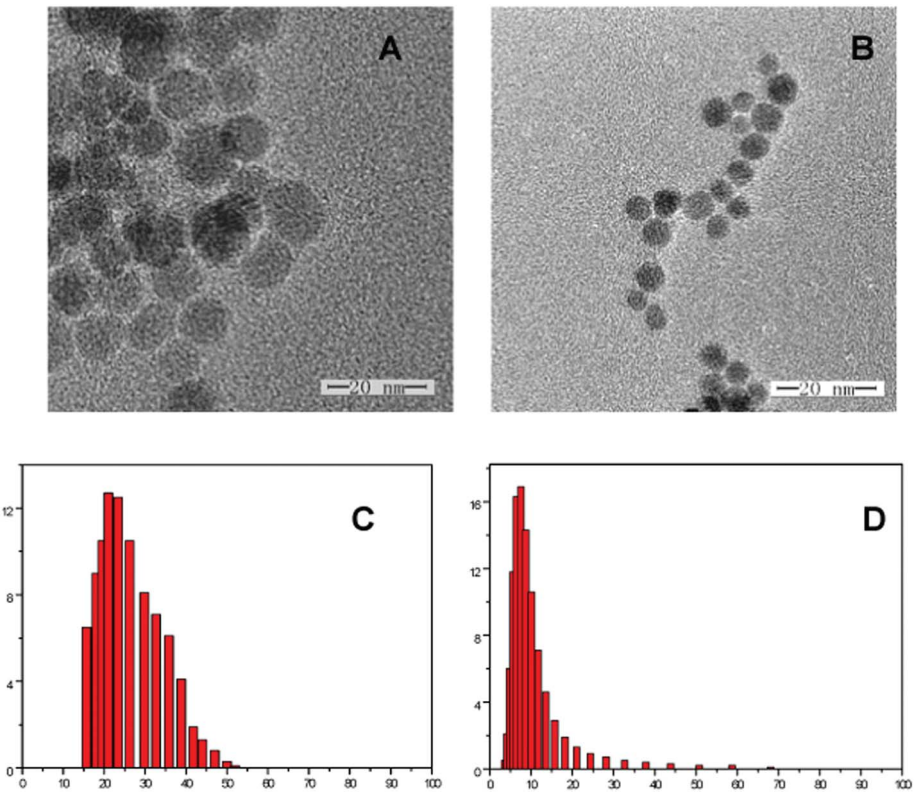

Fig. 2 Size measurements and morphological examination of dex-SPIO and glu-dex SPIO: (A) dex-SPIO; (B) glu-dex SPIO; (C) dex-SPIO, (D) glu-dex SPIO.

SPIO at 24.9 nm ± 1.46 nm (Fig. 2C and D). The different sizes of dex-SPIO and glu-dex SPIO indicated that the hydrophilic glucose may be capable of reducing the nucleation size of the iron oxide particles as well as influencing the thickness of the outer layers of iron oxide crystals.

3.3 Powder X-ray diffraction analysis of the SPIO nanoparticles

Powder X-ray diffraction (XRD) analysis was used to examine the crystalline properties of the SPIO particles (Fig. 3). The XRD patterns of both the dex-SPIO and glu-dex SPIO magnetic nanoparticles were similar with both SPIO exhibiting characteristic peaks that mainly correspond to magnetite (Fe_3O_4) compounds similar to those previously reported.[22,23] Five distinct Fe_3O_4 peaks at 30.1°, 35.5°, 43.1°, 57.0°, and 62.6° accounting for the (220), (311), (400), (511) and (440) crystal planes, respectively, were observed for both SPIO samples. The glu-dex SPIO prepared using the controlled growth co-precipitation process would be expected to be pure magnetite, so it was confirmed that the addition of the proper amount of glucose did not result in a phase change of Fe_3O_4. The XRD analysis also suggests that there is an absence of other nonmagnetic iron oxide species in both dex-SPIO and glu-dex SPIO. The average crystal size, corresponding to the highest intensity peak (311) of the particles, was calculated according to the Scherrer equation. The average particle sizes obtained from the calculation were

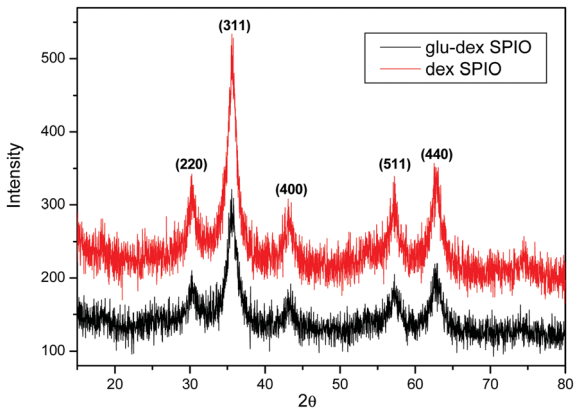

Fig. 3 An overlay of the X-ray power diffraction patterns of dex-SPIO and glu-dex SPIO.

3.5 nm and 7.8 nm for glu-dex SPIO and dex-SPIO, respectively, which are consistent with the TEM experiments.

3.4 Thermal analysis of SPIO

Thermal analysis curves of dex-SPIO and the glu-dex SPIO are shown in Fig. 4. As both of the SPIO samples were obtained by freeze drying, only a slight weight loss occurred from 20 °C to 120 °C due to the evaporation of physically adsorbed water. Apart from the physically adsorbed water loss, the weight loss

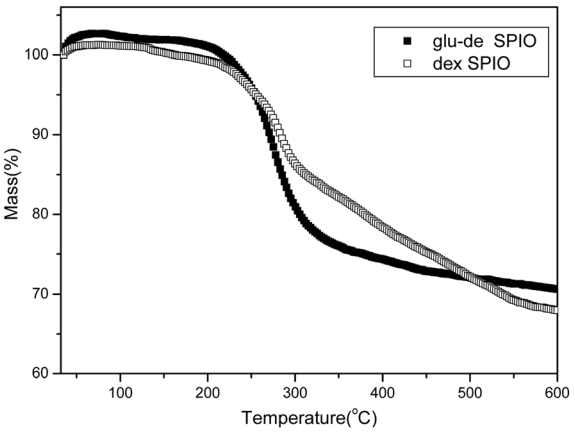

Fig. 4 Thermal gravimetric analysis of dex-SPIO and glu-dex SPIO.

from 120 °C to 300 °C was due to the decomposition of chemically bound water.[24,25] The significant change in the weight loss from 300 °C to 600 °C is the result of the breakdown of molecules on the nanoparticle's surface. From the curve, without the impact of water, it can be calculated that there was a percentage weight loss of 18% for the dex-SPIO particles and 9% for the glu-dex SPIO particles between 300 °C and 600 °C, which can be attributed to the shell of the particles[25] (Fig. 4). As inferred from the smaller weight loss of the glu-dex SPIO sample, the thickness of the shell of the glu-dex SPIO particles should be thinner that of dex-SPIO. The comparison of these results demonstrated the dual function of glucose, which could help control the over growth of the iron oxide core and also help decrease the thickness of the outer layer materials.

3.5 Measurement of the transverse relaxation properties of SPIO

Fig. 5 shows the relationship between $1/T_2$ (y axis) and the concentration of SPIO (x axis). The T_2 relaxation coefficient (r_2) of the SPIO is obtained by measuring the relaxation rate based on the Fe concentration. The r_2 value of dex-SPIO was estimated to be 161.3 mM^{-1} s^{-1} as calculated from the slope of the regression line. The r_2 value of glu-dex SPIO was 130.3 mM^{-1} s^{-1}, which is much higher than that of the commercial T_2 contrast agent Ferumoxtran ($r_2 = 53$ mM^{-1} s^{-1}). It is worthy of note that commercial Ferumoxtran has a similar core size of 4.9 nm and a larger dynamic size of about 22 nm compared to glu-dex SPIO synthesised in this study.[26] As had been previously confirmed, the coating thickness of the SPIO nanoparticles could significantly affect their relaxivity. As the coating thickness increases, the r_2 relaxivity decreases dramatically and our results imply that the relatively higher relaxivity of dex-glu SPIO compared to Ferumoxtran may be attributed to the thinner exterior coating layer.

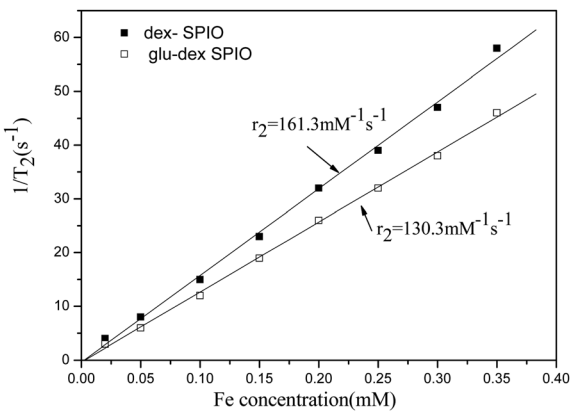

Fig. 5 T_2 relaxation rate ($1/T_2$) as a function of iron concentration of SPIO.

3.6 FA conjugated dex-glu SPIO nanoparticles

A previous study revealed that the signal intensity of normal human synovium remains unchanged after SPIO administration because of the absence of activated macrophages in the healthy synovium.[27] From this standpoint, inflammation site MR imaging might have higher sensitivity and specificity for the evaluation of RA, as even a small signal intensity change would reflect a pathological change. On account of the excellent properties of the glucose and dextran coating method, dex-glu SPIO was selected and conjugated with FA to enhance the MR imaging in an AIA model rat in the following experiments.

The X-ray photoelectron spectroscopy (XPS) spectrum of glu-dex SPIO and FA glu-dex SPIO exhibit similar C1s peaks for their carbon bonds. The major component of the C1s spectrum of dextran coated SPIO at 286.1 eV was primarily due to the CHOH group of the dextran. The broad shoulder observed for glu-dex SPIO could be fitted into three peaks at 284.5, 285.9 and 287.8 eV, which could be attributed to C–C/C–H, C–O and O–C–O, respectively. Two dominant carbon species are expected from dextran, single-bonded C–O and O–C–O in a 5 : 1 ratio (Fig. 6A). These features agree well with reported spectra of dextan coated SPIO.[28–31] After modification, FA glu-dex SPIO showed similar C1s peaks to glu-dex-SPIO at 284.5, 286.0 and 287.8 eV. The relative intensities of these peaks were very close to those of the original glu-dex SPIO. In addition, two typical peaks at 289.0 eV 285.5 eV belonging to C═O and C–N bonds confirmed the incorporation of FA[32] (Fig. 6B). Murine macrophage uptake characterization further confirmed the specific binding effect of the folic acid decorated SPIO. Murine RAW 264.7 macrophages were activated with tumor necrosis factor-α (TNF-α)/interferon (γIFN), and a superior cell uptake efficiency was obtained for FA glu-dex SPIO, whereas a slightly inferior cell membrane penetration effect was observed in glu-dex SPIO (Fig. 7).

3.7 FA Dex-glu SPIO as an MRI contrast agent in AIA rat diagnosis

14 days after a Freund's complete adjuvant injection, the paw scores of the rats suggested that rheumatoid arthritis had developed and immunohistochemical staining was performed in order to confirm the AIA model. A typical example of a hematoxylin–eosin stain of the RA induced using Freund's complete adjuvant, is shown in Fig. 8. As shown in Fig. 8A and B, there are a lot of inflammatory cells immersed in the ankle joint and degeneration or necrosis in the epithelium as well as

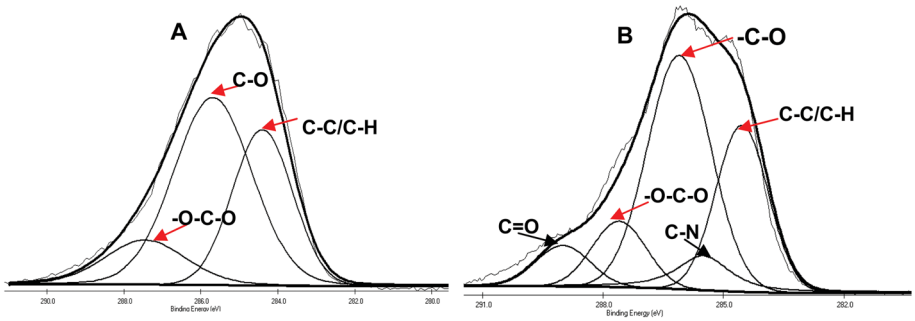

Fig. 6 C1s XPS spectra of glu-dex SPIO (A) and FA glu-dex SPIO (B).

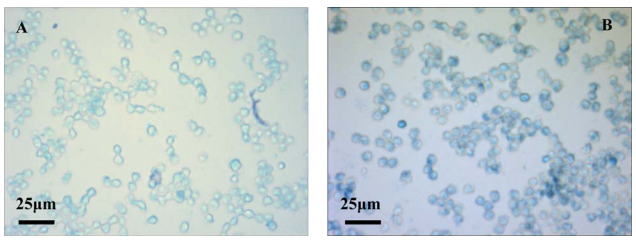

Fig. 7 Cell uptake of SPIO by murine macrophages: (A) glu-dex SPIO; (B) FA glu-dex SPIO.

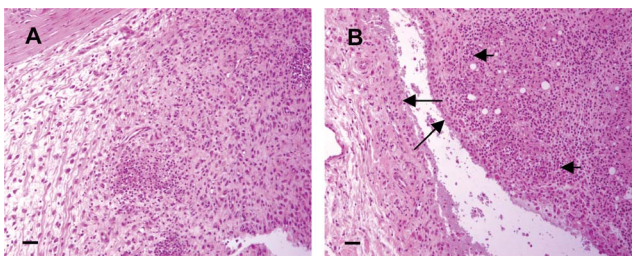

Fig. 8 Photomicrographs of representative hematoxylin and eosin stain sections from an AIA rat: (A) ankle joint; (B) synovium. The long arrow shows the degeneration or necrosis in the epithelium and the short arrow shows the infiltration of inflammatory cells.

infiltration of inflammatory cells observed in the synovium. Immediately thereafter, an MRI scan was performed to investigate the contrast-enhancing capacity of the FA glu-dex SPIO in the detection of AIA rats. Representative T_2-weighted ankle joint images of animals injected with SPIO 24 hours after injection are shown in Fig. 9. Compared with the saline injection control, the FA glu-dex SPIO group image showed a marked negative synovium enhancement and appeared hyperintense compared with the surrounding tissue, which is indicative of SPIO accumulation in these tissues (Fig. 9A and C). On the other hand, the non-targeting SPIO injected rat contained relatively minor signal loss. (Fig. 9A and B). The *in vivo* MRI detection results suggest that the folic acid-conjugated SPIO facilitates access to extravasate through the capillaries and diffuse into the synovium, where folic acid receptors are highly expressed. The ankle join of rat was removed after MR imaging and a histological Prussian blue staining was performed. In agreement with the imaging study, histological analysis demonstrated that a small amount of iron oxide nanoparticles was detected in the joint space with dex-glu SPIO. An increased iron oxide penetration of the synovium was observed for FA dex-glu SPIO (Fig. 9D–F). Overall, the results suggest that folic acid-conjugated iron oxide nanoparticles might be useful as MRI contrast agents for the detection of AIA *in vivo*.

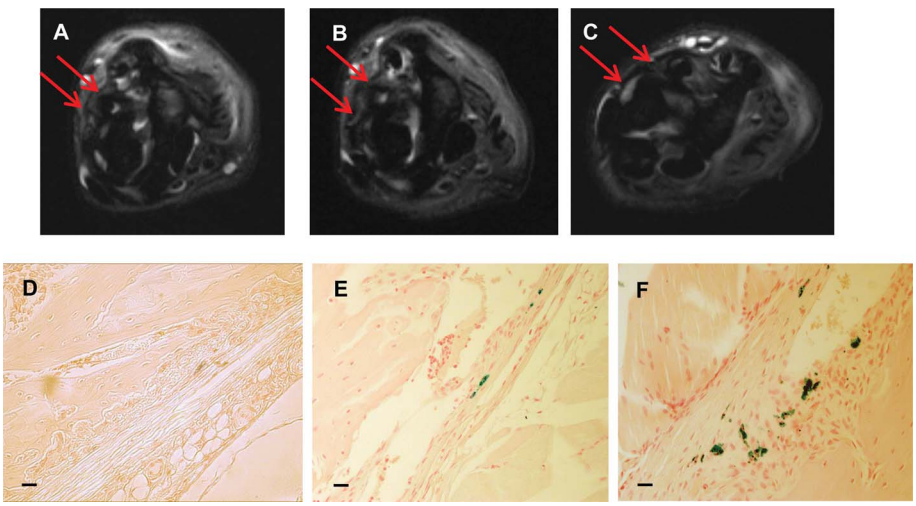

Fig. 9 T_2-weighted MR image and histological Prussian blue staining of AIA rats 24 h post-injection of SPIO: (A) and (D) saline control; (B) and (E) glu-dex SPIO; (C) and (F) FA glu-dex SPIO. The arrow shows the synovium.

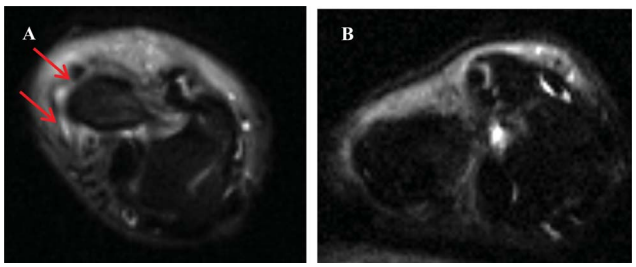

Fig. 10 RA treatment efficacy monitored in AIA rats: (A) control AIA; (B) 10 days later after therapy. The arrow shows the synovium.

3.8. FA Dex-glu SPIO as an MRI contrast agent in AIA rat therapy response

To evaluate the therapeutic response capacity of FA glu-dex SPIO, MR images of AIA rats treated with cyclooxygenase 2 (COX-2) inhibitors were investigated in this section. The rats selected from group had the median degree of AIA and were injected with COX-2 over ten days. At the end of the treatment, T_2-weighted MR images were acquired. The images of the ankle joint before and after COX-2 treatment are shown in Fig. 10. Large areas of marked post contrast enhancement of the synovium were seen in the rat control group, indicating high-grade synovitis (Fig. 10A). As for the ten day COX-2 treatment group, the thickening of the synovium no longer extends along the diaphyses (Fig. 10B), indicating the alleviation of synovitis to some extent. These results suggested that FA glu-dex SPIO might be useful as a contrast agent for quantifying the recovery level of the synovium of rheumatoid arthritis.

4 Conclusion

\In conclusion, the present results demonstrated that glu-dex SPIO decorated with FA is an excellent agent for the enhancement of contrast in the inflamed joints of a rat model of rheumatoid arthritis. Significant differences between the synovium and adjacent tissue were obtained for FA glu-dex SPIO and non-targeting SPIO in AIA rats using 7 T MRI. In addition, FA glu-dex SPIO nanoparticles have proven to be more sensitive than non-targeting SPIO for detecting the outcome of COX-2 treatment. Therefore, FA glu-dex SPIO particles are not only potential contrast agents for diagnosis, but allow us to evaluate long term response to anti-rheumatic drugs in rheumatoid arthritis treatment.

Acknowledgements

This work was financially supported by the National Natural Science Foundation of China (Grant no. 21304099, 51203162, 51103159, 51373177), the National High Technology Research and Development Program (Grant no. 2014AA020708, 2012AA022703, 2012AA020804), the Instrument Developing Project of the Chinese Academy of Sciences (Grant no. YZ201253, YZ201313), the Open Funding Project of the National Key Laboratory of Biochemical Engineering (Grant no. Y22504A169) and the "Strategic Priority Research Program" of the Chinese Academy of Sciences, (Grant no. XDA09030301-3).

References

1 V. M. Rantalaiho, H. Kautiainen, M. Korpela, P. J. Hannonen, M. Leirisalo-Repo, T. Mottonen and F.-R. T. Grp, *Ann. Rheum. Dis.*, 2013, **72**, 786–788.
2 A. Guin, M. C. Adhikari, S. Chakraborty, P. Sinhamahapatra and A. Ghosh, *Semin. Arthritis Rheum.*, 2013, **43**, 48–54.
3 B. A. Nguyen-Khoa, E. L. Goehring, K. A. Alexander, W. Dong, P. Napalkov and J. K. Jones, *Semin. Arthritis Rheum.*, 2013, **42**, 450.
4 L. C. Vasanth, H. Pavlov and V. Bykerk, *Rheumatic Diseases Clinics of North America*, 2013, **39**, 547–566.
5 M. Boesen, M. Ostergaard, M. A. Cimmino, O. Kubassova, K. E. Jensen and H. Bliddal, *Eur. J. Radiol.*, 2009, **71**, 189–196.
6 A. Giovagnoni, G. Valeri, E. Burroni and F. Amici, *Eur. J. Radiol.*, 1998, **27**, S25–S30.
7 T. Suzuki, S. Ito, S. Handa, K. Kose, Y. Okamoto, M. Minami, T. Hayashi, D. Goto, I. Matsumoto and T. Sumida, *Mod. Rheumatol.*, 2009, **19**, 358–365.
8 B. C. te Boekhorst, L. B. Jensen, S. Colombo, A. K. Varkouhi, R. M. Schiffelers, T. Lammers, G. Storm, H. M. Nielsen, G. J. Strijkers, C. Foged and K. Nicolay, *J. Controlled Release*, 2012, **161**, 772–780.
9 J. F. Lutz, S. Stiller, A. Hoth, L. Kaufner, U. Pison and R. Cartier, *Biomacromolecules*, 2006, **7**, 3132–3138.
10 M. De Cuyper, S. J. Soenen, K. Coenegrachts and L. T. Beek, *Anal. Biochem.*, 2007, **367**, 266–273.
11 E. K. U. Larsen, T. Nielsen, T. Wittenborn, H. Birkedal, T. Vorup-Jensen, M. H. Jakobsen, L. Ostergaard, M. R. Horsman, F. Besenbacher, K. A. Howard and J. Kjems, *ACS Nano*, 2009, **3**, 1947–1951.
12 C. C. Berry, S. Wells, S. Charles and A. S. Curtis, *Biomaterials*, 2003, **24**, 4551–4557.
13 K. G. Paul, T. B. Frigo, J. Y. Groman and E. V. Groman, *Bioconjugate Chem.*, 2004, **15**, 394–401.
14 A. Bumb, M. W. Brechbiel, P. L. Choyke, L. Fugger, A. Eggeman, D. Prabhakaran, J. Hutchinson and P. J. Dobson, *Nanotechnology*, 2008, **19**, 335601–335606.
15 Z. G. Estephan, H. H. Hariri and J. B. Schlenoff, *Langmuir*, 2013, **29**, 2572–2579.
16 L. Babes, B. Denizot, G. Tanguy, J. J. Le Jeune and P. Jallet, *J. Colloid Interface Sci.*, 1999, **212**, 474–482.
17 B. R. Jarrett, M. Frendo, J. Vogan and A. Y. Louie, *Nanotechnology*, 2007, **18**, 035603–035609.
18 S. J. Bae, J. A. Park, J. J. Lee, G. H. Lee, T. J. Kim, D. S. Yoo and Y. M. Chang, *Curr. Appl. Phys.*, 2009, **9**, S19–S21.
19 T. Matsushita, Y. Kusakabe, H. Fujii, K. Murase, Y. Yamazaki and K. Murase, *Magn. Reson. Imaging*, 2011, **29**, 173–178.
20 P. S. Low, W. A. Henne and D. D. Doorneweerd, *Acc. Chem. Res.*, 2008, **41**, 120–129.
21 L. Zhou, Y. L. Yu, L. Chen, P. Y. Zhang, X. L. Wu, Y. S. Zhang, M. Yang, J. Di, H. Y. Jiang and L. Y. Wang, *J. Immunol. Methods*, 2012, **386**, 78–84.

22 S. L. Easo and P. V. Mohanan, *Carbohydr. Polym.*, 2013, **92**, 726–732.
23 P. Kucheryavy, J. B. He, V. T. John, P. Maharjan, L. Spinu, G. Z. Goloverda and V. L. Kolesnichenko, *Langmuir*, 2013, **29**, 710–716.
24 M. Mikhaylova, D. K. Kim, C. C. Berry, A. Zagorodni, M. Toprak, A. S. G. Curtis and M. Muhammed, *Chem. Mater.*, 2004, **16**, 2344–2354.
25 T. J. Chen, T. H. Cheng, C. Y. Chen, S. C. Hsu, T. L. Cheng, G. C. Liu and Y. M. Wang, *JBIC, J. Biol. Inorg. Chem.*, 2009, **14**, 253–260.
26 C. W. Jung and P. Jacobs, *Magn. Reson. Imaging*, 1995, **13**, 661–674.
27 S. Lefevre, D. Ruimy, F. Jehl, A. Neuville, P. Robert, C. Sordet, M. Ehlinger, J. L. Dietemann and G. Bierry, *Radiology*, 2011, **258**, 722–728.
28 C. W. Jung, *Magn. Reson. Imaging*, 1995, **13**, 675–691.
29 S. P. Massia and J. Stark, *J. Biomed. Mater. Res.*, 2001, **56**, 390–399.
30 R. A. Frazier, M. C. Davies, G. Matthijs, C. J. Roberts, E. Schacht, S. J. B. Tendler and P. M. Williams, *Langmuir*, 1997, **13**, 7115–7120.
31 U. Janciauskaite, V. Rakutyte, J. Miskinis and R. Makuska, *React. Funct. Polym.*, 2008, **68**, 787–796.
32 C. Huang, K. G. Neoh and E. T. Kang, *Langmuir*, 2012, **28**, 563–571.